Evaluation of Modular Integrated Electric Drive Concepts for Automotive Traction Applications

Hui Zhang, *Student Member, IEEE*, Lebing Jin, *Student Member, IEEE*,
Oskar Wallmark, *Member, IEEE*, and Staffan Norrga, *Member, IEEE*

***Abstract*—In order to achieve compactness and realize a certain level of fault tolerance in integrated motor drives (IMDs), a number of integrated modular motor drive (IMMD) concepts have been proposed in recent years. In this paper, converter topology candidates suitable for an IMMD are considered with particular focus on the stacked polyphase bridges converter, the parallel-connected polyphase bridges converter, and the modular high frequency converter. A comparative evaluation of the studied topologies is presented and discussed in terms of machine design aspects, power losses, capacitor energy storage requirements, costs, and cell redundancy using the conventional two-level three-phase drive system as reference.**

***Index terms*—** Electric vehicles, integrated motor drives, modular converters, permanent magnet machines.

I. Introduction

By integrating the power converter with the electric machine, a compact electric drive can potentially be realized that meets the requirements in terms of power density and efficiency that are called for in automotive applications. Compared to when the machine and corresponding power electronics are two separate units, having the power electronics close to the machine (e.g., inside the same housing) offers a number of benefits, including reduced cabling and potential reductions in terms of electromagnetic interference (EMI) and volume requirements [1]–[4].

In recent years, integrated motor drives (IMDs) have been employed in a number of industrial [5]–[7] and traction applications [8]–[10]. Broadly, these IMDs can be categorized according to the physical position of the power converter: surface-mount integration (depicted in Fig. 1 (a)) and axial-end-mount integration (depicted in Figs. 1 (b)–(c)). In surface mount IMDs, the power converter is integrated in or situated on the surface of the machine casing, a solution attractive due to its simplicity and low cost [11]. In an axial-end mount IMD, the power converter is mounted on the axial end (non-drive side) of the machine, either on the external surface of the end-plate of the machine casing (Fig. 1 (b)) or within the axial-end interior of the machine casing (Fig. 1 (c)). The latter is a potentially more compact solution but careful thermal analysis is required due to the reduced thermal barrier between the machine and the power converter [2], [4].

Relatively recently, integrated *modular* motor drives (IMMDs) have started to be considered for automotive traction applications. Here, the modularity is realized by functionally replacing the conventional three- or multi-phase converter with several modularized drive units where each unit comprises of part of the electric machine and its corresponding converter and bus capacitance. Fig. 2 (a) depicts an IMMD solution realized by physically separating a five-phase drive into five phase-leg units equipped with associated power electronics [12], [13]. Another solution, shown in Fig. 2 (b), utilizes series- or parallel-connected modular-concept converters [14]–[21] and offers submodule-level redundancy and the possibility to eliminate certain harmonics in the dc-link current by adopting interleaving of the modulation carriers [18], [20], [22].

H. Zhang, L. Jin, O. Wallmark and S. Norrga are with the Department of Electric Power and Energy Systems, Electrical Engineering, KTH Royal Institute of Technology, SE-100 44 Stockholm, Sweden (e-mail: lebingj@kth.se; huizhang@kth.se; owa@kth.se; norrga@kth.se).

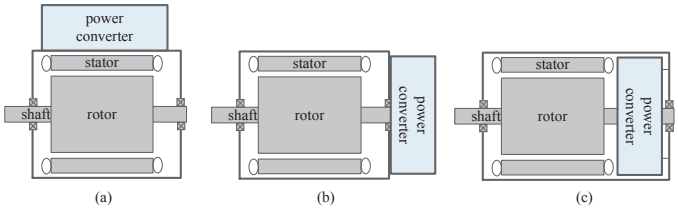

Fig. 1. Alternatives for power converter integration: (a) surface mount; (b) end-plate mount; (c) within axial-end interior mounting.

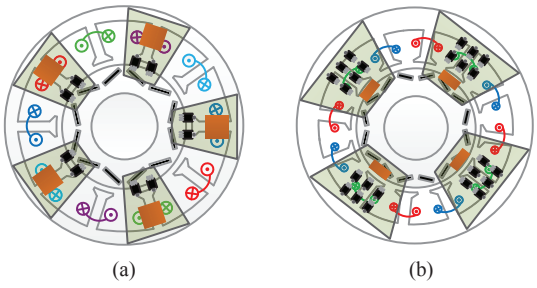

Fig. 2. Sample IMMD concepts: (a) phase-leg inverter [12], [13]; (b) modular-concept converter [14]–[21].

To realize a fair comparison between different IMMD concepts, the corresponding electric machine has to be considered as well. As summarized in Table I, induction machines (IMs) and permanent-magnet synchronous machines (PMSMs) are commercially favorable [23]. From the investigation in [24], however, PMSMs with interior mounted permanent magnets, here abbreviated IPMs, are found to be the most suitable machine type when aiming at fulfilling the FreedomCar 2020 specifications and IPMs are, therefore, considered also in this paper.

TABLE I
SAMPLE ELECTRIC VEHICLE MODELS IN THE MARKET.

Model	EM type	Max. power [kW]	Year
Nissan Leaf Acenta	PMSM	80	2016
Fiat 500e	PMSM	83	2015
Chevy Spark EV	PMSM	105	2015
Ford Focus Electric	PMSM	107	2015
Kia Soul EV	PMSM	81	2015
Mercedes-Benz B250e	IM	132	2015
Tesla ModelS 60	IM	225	2015
Toyota RAV 4 EV	IM	115	2014
BMW i3	PMSM	125	2014
Honda Fit EV	PMSM	92	2014
Mitsubishi i-MiEV	PMSM	49	2014
Volkswagen e-up!	PMSM	85	2013

Stator windings sectioned into a number of modules with each corresponding converter unit placed closely enables a tight machine-converter integration [25]. Fractional-slot concentrated windings (FSCWs) provide relatively independent coil-units to connect with the associated converter units and when compared to integer-slot distributed windings (ISDWs), FSCWs also have shorter end-turns and higher fill factors can be achieved [26]–[28]. However, FSCWs exhibit a higher content of space harmonics which particularly increases the rotor losses [26]. In addition, for IPMs, the effective rotor saliency is generally lower with FSCWs than with ISDWs [27]. Therefore, FSCWs require a higher stator flux magnitude for a given torque level which particularly reduces the efficiency during high-speed operation compared to a corresponding ISDW.

A. Contribution and Outline of Paper

From the references above, it is clear that a considerable amount of work is ongoing towards realizing very compact integrated electric drives for automotive applications. An overall aim and novel contribution of this paper is the comparison of recently proposed IMMD concepts taking into account aspects of *both* electric machine design *and* power electronics simultaneously. Particularly, the investigation is focused on the stacked polyphase bridges (SPB) topology, the parallel-connected polyphase bridges (PPB) topology and the modular high frequency (MHF) topology which all are compared to the conventional two-level three phase converter. Using the FreedomCar 2020 specifications as a starting point, electric machinery suitable for the different converter topologies are designed and compared in weight, volume, fault tolerance, and cost (thermal management and packaging technologies are not addressed in this paper). For the corresponding power switch devices, the resulting losses, capacitor energy storage requirements and cost for the different modular converter concepts are then presented taking into account both silicon devices (Si IGBT and Si MOSFET) and wide-bandgap devices (SiC MOSFET and GaN FET).

The paper is outlined as follows. In Section II, four alternative converter topologies in IMMDs for EV/HEV applications are introduced along with their particular advantages and associated control strategies. Machine topologies and corresponding winding arrangements are discussed in Section III. In Section IV, three targeted IPM-FSCW machines and a conventional three-phase IPM machine with distributed windings are designed based on the same specification. Corresponding suitable converters are devised based on the resulting machine parameters. Moreover, the overall system performance, including cost, over-loading and cell redundancy are evaluated. Finally, concluding remarks are provided in Section V.

II. CONVERTER TOPOLOGIES FOR IMDS

A. Conventional Two-Level Converter

A typical electric drive in EVs comprises of a battery, a dc-link capacitor, a three-phase two-level converter and a corresponding three-phase electric machine. As depicted in Fig. 3, such a two-level converter consists of three phase legs that are connected to a common dc-link capacitor. Each phase leg includes two semiconductor switches with anti-parallel diodes. In automotive applications, the converter should provide three-phase voltages of variable amplitude and frequency from a dc bus voltage which is normally in the range 300 V–600 V. Hence, 600 V–1200 V silicon IGBTs are commonly used as semiconductor switches which limits the switching frequency to below around 30 kHz. The assembly of the required dc-link capacitor usually takes up around 30% of the total converter volume which makes a compact integration of the conventional two-level converter and electric machine challenging [29].

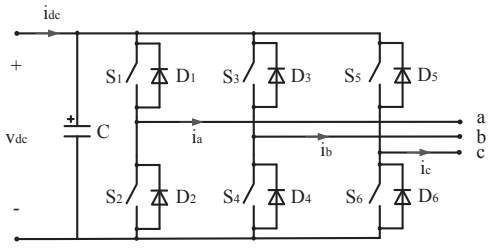

Fig. 3. Two-level three-phase converter topology.

B. Alternative Converter Topologies

In order to increase compactness and reliability of IMDs, alternative converter topologies have started to be considered also for automotive applications. In general, these topologies enable a smaller dc-link capacitance and a certain level of fault tolerance. Four promising topologies are briefly reviewed in this section.

1) Stacked Polyphase Bridges Converter: The stacked polyphase bridges (SPB) converter comprises of a number of series-connected *submodules*, each consisting of a two-level converter with its corresponding capacitor (see Fig. 4). The ac terminals of each submodule can be connected to one set of three-phase windings of a multi-phase machine [25]. Apart from other common benefits of modular converters, a key advantage of the SPB concept is that the topology allows the use of low-voltage semiconductors such as silicon MOSFETs or gallium nitride FETs. As these semiconductors allows for higher switching frequencies and can withstand high maximum junction temperatures, this enables submodules with

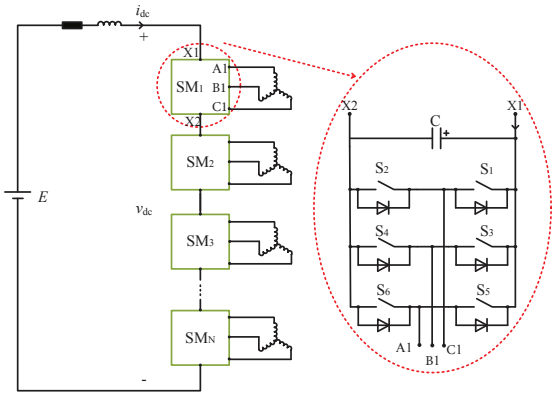

Fig. 4. Basic structure of the SPB converter.

small dc capacitances, potentially sharing the same housing as the corresponding electric machine.

Since the submodules are connected in series, a dc voltage control is necessary. In order to balance the dc voltages on each submodule, the dc-link stability controllers proposed in [18], [30], [31] aim to adjust each submodule dc voltage according to its reference (which normally is the average value of all capacitor voltages). On each submodule, a standard vector current controller for conventional two-level converters can then be adopted (e.g., the one presented in [32]).

2) Parallel-Connected Polyphase Bridges Converter: Two types of parallel-connected polyphase bridges (PPB) converters, PPB-I and PPB-II are considered here and they are described below.

- PPB-I: Designated as PPB-I is a conventional multiphase converter (see Fig. 5). When being a part of an IMMD system, each phase leg together with the associated power electronics can be assembled as a single unit [33]. Compared to three-phase drive systems, increasing the number of phases reduces low-frequency torque ripple and, with proper control, post-fault operation in the event of a phase-leg failure can be realized [34]–[36]. Since the number of phases is increased, the current rating of each phase leg is reduced which simplifies the integration. The same vector control scheme as for a conventional three-phase drive system can be used with the only difference that the coordinate transformation (*abc*–*dq* transformation) needs to produce m_{ph} phase voltage references (m_{ph} being the number of phases) [37].
- Type II: PPB-II is illustrated in Fig. 6. As seen, it comprises of several two-level three-phase converters connected in parallel. Similar to the SPB converter, each submodule comprises of three phase legs and an associated dc capacitor [20], [38]. By interleaving the PWM carriers in the submodules, the required submodule capacitance can be minimized.

3) Modular High Frequency Converter: The modular high frequency converter (MHF) represents another path towards realizing a modular integration of the power converter with the electric machine [39]. As depicted in Fig. 7, each submodule of the MHF converter consists of a step-up converter and an H-bridge, both connected to a common dc capacitor. The H-bridge outputs a single-phase ac voltage which can feed one phase of the electric machine. Similar to the SPB topology, the series connection of each submodule allows the use of low-voltage FETs.

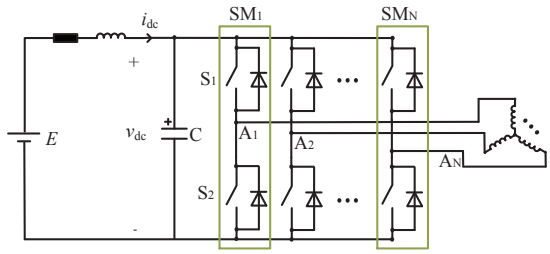

Fig. 5. Basic structure of the PPB-I converter.

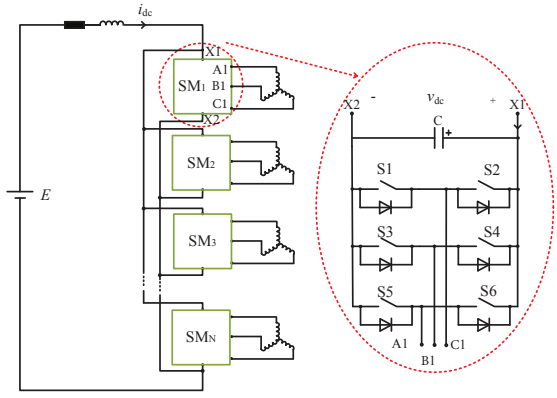

Fig. 6. Basic structure of the PPB-II converter.

In each submodule, the internal supply voltage v_{cap} is controlled to a given value by adjusting the duty cycle of the step-up converter [40]. Due to the single-phase output, the power flow from the H-bridge contains a second-order fluctuation which can be suppressed by varying the duty cycle of the step-up converter as described in [41].

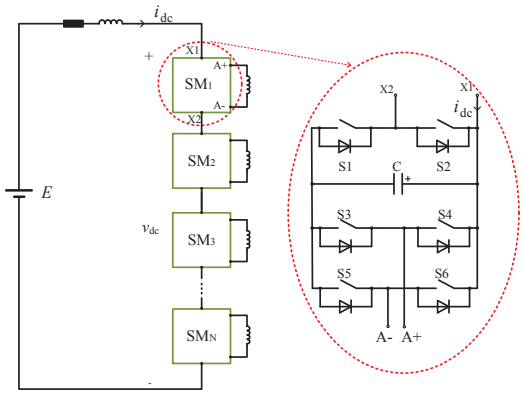

Fig. 7. Basic structure of the MHF converter.

III. Modular Electric Machinery

The converter and machine combination considered as a reference case in this paper comprises of an IPM-ISDW machine and a three-phase two level converter. To comply

with the converter topologies suitable for IMMDs, three IPM-FSCW machines have been selected following the machine-converter integration guidelines in [25]. For the SPB- and MHF-type converters, an eight-pole, three-phase IPM-FSCW machine with 12 slots and a six-pole, five-phase IPM-FSCW machine with 10 slots are selected, respectively. The same IPM-FSCW machine as for the SPB-type converter is also used for the PPB-II converter (utilizing a number of three-phase converters connected in parallel) but the number of turns are adjusted to comply with the increased voltage. The cross-sectional views of the three machines are displayed in Fig. 8.

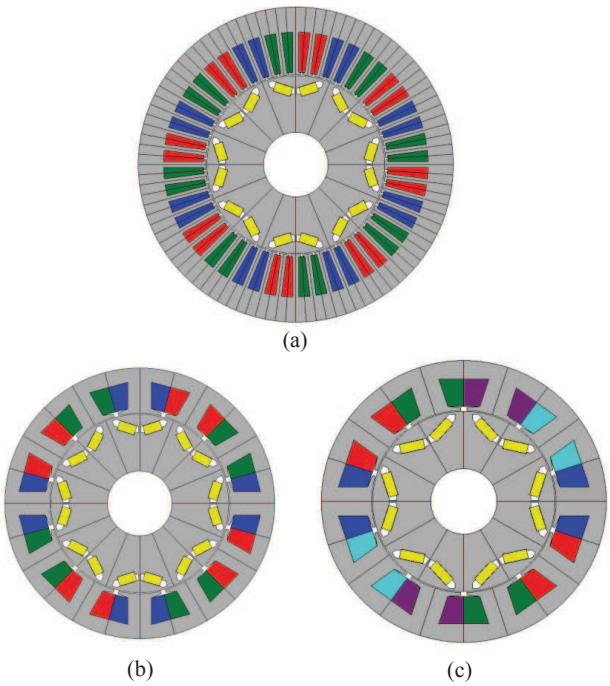

Fig. 8. Cross-sectional views of: (a) conventional three-phase IPM-ISDW machine with 48 slots and 8 poles; (b) three-phase IPM-FSCW machine with 12 slots and 8 poles for the SPB- and PPB-II converter; (c) five-phase IPM-FSCW machine with 10 slots and 6 poles for the MHF- and PPB-I converter.

Each submodule of the MHF and PPB-I converter is connected to the coils belonging to the same phase. Therefore, for these two converters the number of converter submodules m_{sm} is selected equal to the number of phases $m_{\mathrm{ph}} = 5$. On the contrary, each SPB and PPB-II converter submodule is connected to a set of three- or multi-phase coils. For the corresponding stator winding depicted in Fig. 8 (b), the winding periodicity $t_{\mathrm{per}} = 4$ (see [42]) meaning that the stator winding can be divided into four equivalent sets of three-phase coils. Therefore, the number of submodules m_{sm} is selected as $m_{\mathrm{sm}} = t_{\mathrm{per}} = 4$ [25]. The resulting winding arrangements of these three IPM-FSCW machines and the connection to the associated converter submodules are depicted in Figs. 9-10.

IV. System Design and Evaluation

Table II shows the adopted FreedomCar 2020 design specifications obtained from [26], [27], [42]–[44]. The dc-link

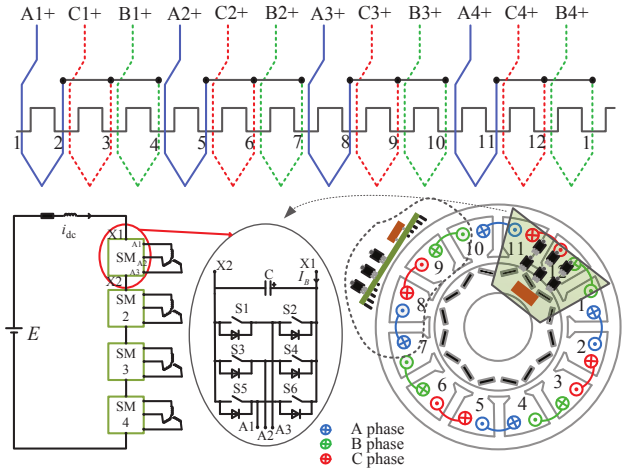

Fig. 9. IMD with an SPB converter (same winding layout for the PPB-II converter but adjusted number of turns to account for the increase in voltage).

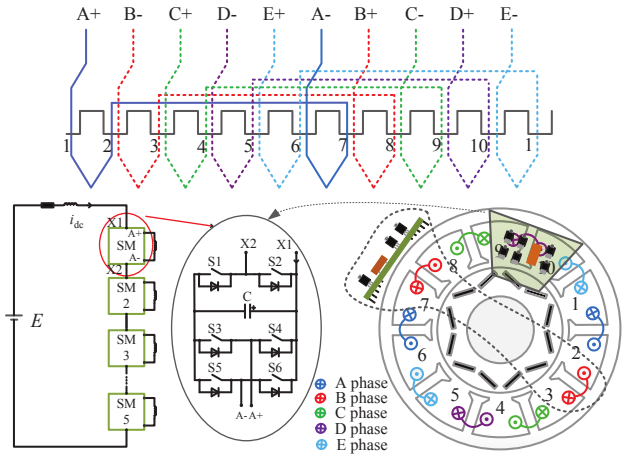

Fig. 10. IMD with an MHF converter (same winding layout for the PPB-I converter but adjusted number of turns to account for the increase in voltage).

voltage V_{dc} can be chosen from 200 V to 450 V [27]. For the conventional-, SPB- and PPB-type converter, a rated dc-link voltage of $V_{\mathrm{dc}} = 400$ V ensures relatively moderate current- and voltage-ratings when selecting available semiconductors and is, therefore, used as the dc bus voltage in this work. $V_{\mathrm{dc}} = 250$ V is selected for the MHF converter to ensure a 100 V capacitor voltage v_{cap} enabling similar voltage ratings for the semiconductors as for the SPB-type converter.

Remark: It should be empathized that fulfilling all FreedomCar 2020 specifications must be considered very demanding [44] and this is not claimed in this work. Rather, the designs presented in this work highlight the relative differences that the different modular concepts result into.

A. Machine Design and Analysis

Based on the specifications in Table II, three candidate electric machines have been designed following the iterative finite-element design approach described in [45] using the software JMAG[1]. During this design process, the parameters listed below are kept constant.

[1]JMAG is a registered trademark of the JSOL Corporation, Tokyo, Japan.

TABLE II
FREEDOMCAR 2020 TRACTIVE DRIVE SPECIFICATION.

Electric machine		
Specification	Unit	Target
Rated speed	[rpm]	2800
Maximum speed	[rpm]	14000
Continuous power	[kW]	30
Peak power	[kW]	55
Mass (with frame)	[kg]	$\leq$35
Volume (with frame)	[L]	$\leq$9.7
Unit cost	[$]	$\leq$275
Power electronics		
Power density	[kW/kg]	$\leq$ 1.6
Cost	[$/kW]	$\leq$ 4.7

- The inner diameter of the stator D_{si} is kept fixed to $D_{\text{si}} = 140$ mm;
- The air-gap length δ is fixed to $\delta = 0.75$ mm;
- The peak-fundamental air-gap flux density at no load $\hat{B}_\delta$ is fixed to $\hat{B}_\delta \approx 0.6$ T in order to avoid over-saturating the stator core during peak torque operation;
- The *characteristic current* $\hat{I}_{\text{ch}}$, defined as the ratio of the magnet flux linkage ψ_m to the d-axis inductance L_d [26]

$$\hat{I}_{\text{ch}} = \frac{\psi_m}{L_d} \tag{1}$$

  is designed to be approximately equal to the rated current ($\hat{I}_{\text{ch}} \simeq \hat{I}$) for all three machines in order to obtain a wide speed range [46]. This also indicates that the designs are fault-tolerant in the sense that steady-state current during a balanced short circuit of a submodule is equal to rated current.
- A detailed thermal analysis of the resulting machine designs is not considered in this work. Therefore, the continuous and maximum conductor current density are set to 10 and 20 Arms/mm^2, respectively which are values commonly found in water-cooled electric machinery.

The resulting three candidate machines are labeled M1–M3 and key parameters are reported in Table III.

1) Volume and Mass: The stack lengths of the IPM-FSCW machines (M2–M3) are longer than the stack length of the IPM-ISDW machine (M1) which partly can be attributed to the smaller effective rotor saliency [47]. However, the IPM-ISDW machine (M1) has a larger outer stator diameter and more copper is required due to the lower fill factor (0.35 and 0.46 assumed for ISDW and FSCW, respectively) and the longer end-turn lengths [28]. By assuming the arc of an end-turn to be circular (following [48]), the axial build of an end-turn can be estimated. Fig. 11 indicates that all three machines should fulfill the FreedomCar 2020 volume requirement. The volume of the end-turns account for almost 50% of the total volume of the IPM-ISDW machine (M1) and the total volume of M1 is the largest, despite its shortest stack length. As reported in Table III, the predicted active weights of M1–M3 are in the range 26.5–31.5 kg. It could, hence, be questioned whether the total weight (including a water cooled frame) would fulfill the FreedomCar 2020 weight requirement. Nevertheless, the resulting designs highlight the relative differences in weight and volume that the different modular concepts result into.

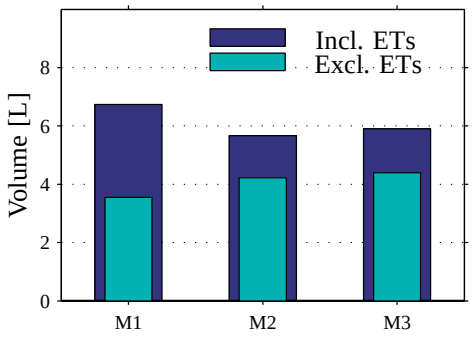

Fig. 11. Comparison of predicted electric machine volumes including and excluding the end-turns (ETs).

2) Flux Weakening: The resulting torque-speed and power-speed curves at continuous operation are shown in Fig. 12 and Fig. 13, respectively. From Fig. 13, the constant power speed range (CPSR) is approximately 3 to 4 for M1–M3 and all designs fulfill the maximum speed requirement of 14000 rpm in Table II. Fig. 14 shows that all three machines approximately fulfill the design requirement of 30 kW continuous power at rated speed (2800 rpm). The peak power, defined as the maximum power output at rated speed with a conductor current density of 20 Arms/mm^2 also approximately reaches the required 55 kW.

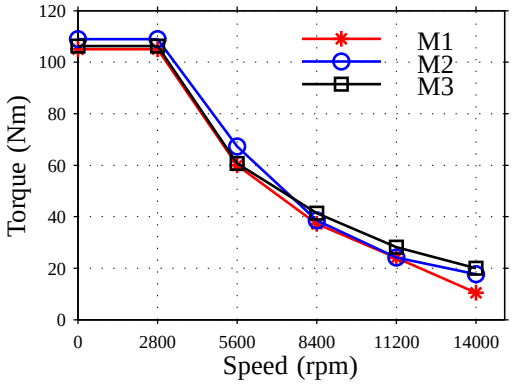

Fig. 12. Torque-speed characteristics (continuous operation).

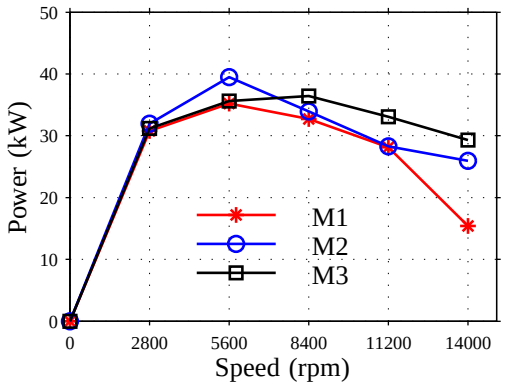

Fig. 13. Power-speed characteristics (continuous operation).

TABLE III
IPM PARAMETERS.

Converter type	Unit	Conv.	SPB	PPB-II	PPB-I	MHF
Converter connection	-	-	Series	Parallel	Parallel	Series
Machine	-	M1	M2		M3	
# phases	-	3	3		5	
# slots	-	48	12		10	
# poles	-	8	8		6	
m_{sm}	-	1	4		5	
Stator outer diameter	[mm]	245.5	210.0		215.9	
Stator inner diameter	[mm]	140	140		140	
Stack length	[mm]	75	122		122	
End-turn axial build	[mm]	33.6	20.8		20.9	
Air-gap length	[mm]	0.75				
PM type	-	NdFeB				
PM relative permeability	-	1.04				
Coercive force	[kA/m]	925				
Magnet thickness	[mm]	7.2				
Magnet width	[mm]	13.7	13.7		18.4	
Stator core mass	[kg]	12.29	11.93		13.49	
Rotor core mass	[kg]	6.19	10.06		10.06	
PM mass	[kg]	0.93	1.52		1.53	
Copper mass	[kg]	5.85	4.04		4.47	
Shaft mass	[kg]	1.23	2.0		2.0	
Total mass	[kg]	26.46	29.55		31.54	
Rated phase rms current	[Arms]	89.7	85.8	21.5	55.9	116.8
Characteristic rms current	[Arms]	89.0	84.7	21.2	55.8	116.7
Power factor	-	0.74	0.71		0.75	
# turns of per slot	-	8	24	96	46	22

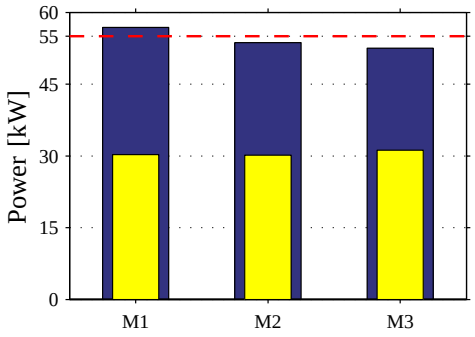

Fig. 14. Continuous power (yellow bar) and peak power (blue bar) at rated speed (2800 rpm).

B. Power Losses of Modular Converters

Seven commercially available semiconductor devices are selected for evaluation of resulting losses when used in the converter topologies reviewed in Section II. Table IV reports main information of these devices. For comprehensiveness, the devices include conventional silicon semiconductors as well as wide band-gap (WBG) alternatives, such as SiC and GaN devices. The 150 V devices are suitable for the SPB and MHF converters utilizing series connected submodules whereas the 650 V devices are considered for the conventional two-level converter as well as the PPB-I and PPB-II converters. Since the semiconductor devices have different current ratings, in order to make a fair loss comparison a different number of devices needs to be paralleled to effectively form one switch with the same current ability.

The loss models used for the calculation adopt the methods presented in [49] and [50] and a switching frequency of 30 kHz is assumed in all cases. Fig. 15 shows the predicted converter losses as a function of normalized semiconductor area[2] A for all combinations of converter topology and semiconductor device. As can be seen, the PPB-I and PPB-II converters result in similar losses as the conventional two-level converter, dissipating around 0.5–3% of losses. The SPB and MHF converters both result in relatively high losses when considered with silicon devices whereas significantly lower losses are achieved with WBG devices.

Considering the overloading requirements common in EV/HEV traction applications, the required total number of devices for each configuration and the corresponding semiconductor cost when $A = 3$ are reported in Fig. 16. The reduction in losses but higher cost of today's WBG-device based switches compared to silicon is clearly reflected. Further, since the WBG devices have relatively low current ratings, a larger number of devices is required compared to silicon.

Remark: Device #1 comprises of six IGBTs together with associated drive circuits and represents, hence, a complete two-level three-phase converter.

C. Energy Storage Requirements

As mentioned, a large/bulky dc-link capacitance aggravates the realization of a compact IMD system. Based on the electrical model of an automotive Li-ion battery presented in [52], Fig. 17 shows the capacitor energy-storage requirements τ as function of switching frequency for the four studied converter

[2] A is defined as $A = N_d/N_{\text{base}}$ where N_d is the total number of semiconductor chips and N_{base} is the minimum number of semiconductor chips required for the rated phase current. For example, $A = 2$ means that with N_d devices in total, the converter can handle a maximum of twice the rated phase current.

TABLE IV
POWER SEMICONDUCTOR DEVICE ALTERNATIVES.

♯	Type	Model no.	Unit price [51] [$]	$V_{\max}$ [V]	I_{nom} [A]	Suitable converter
1	Si IGBT	FS400R07A1E3H5	452.21	650	400	Conv.
2	Si IGBT	IKW50N65F5A	3.94	650	50	PPB
3	Si MOSFET	IPW65R048CFDA	10.85	650	63	Conv./PPB
4	Si MOSFET	AUIRFP4568	5.26	150	171	SPB/MHF
5	SiC MOSFET	SCT2120AF	7.89	650	29	Conv./PPB
6	GaN FET	GS66516T	50.57	650	60	Conv./PPB
7	GaN FET	EPC2033	4.10	150	31	SPB/MHF

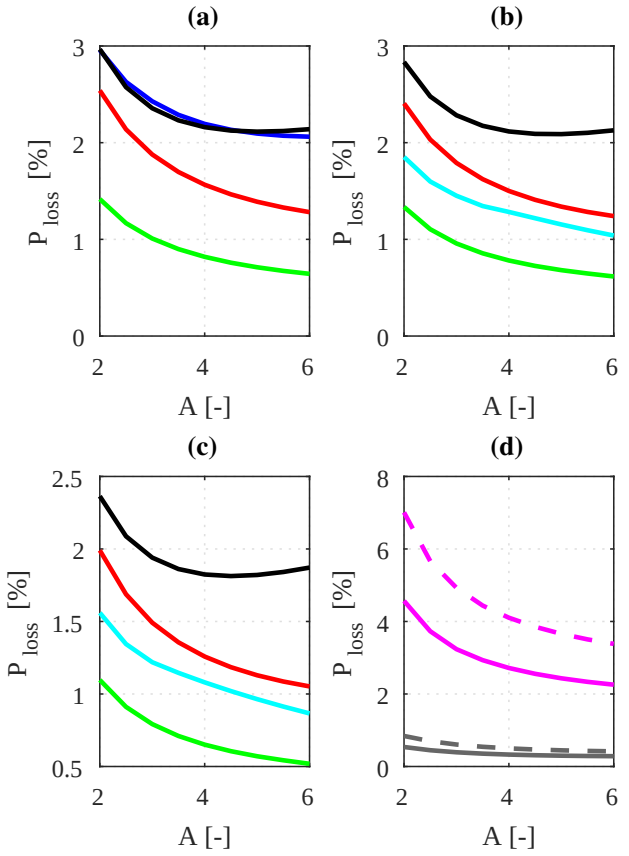

Fig. 15. Loss comparison for the conventional two-level converter and four alternative converters implemented with different semiconductor devices (assuming a switching frequency of 30 kHz): (a) blue: Conventional–#1 (device # refer to Table IV), black: Conventional–#3, red: Conventional–#5, green: Conventional–#6; (b) cyan: PPB-I–#2, black: PPB-I–#3, red: PPB-I–#5, green: PPB-I–#6; (c) cyan: PPB-II–#2, black: PPB-II–#3, red: PPB-II–#5, green: PPB-II–#6; (d) magenta: SPB–#4, gray: SPB–#7, dashed magenta: MHF–#4, dashed gray: MHF–#7.

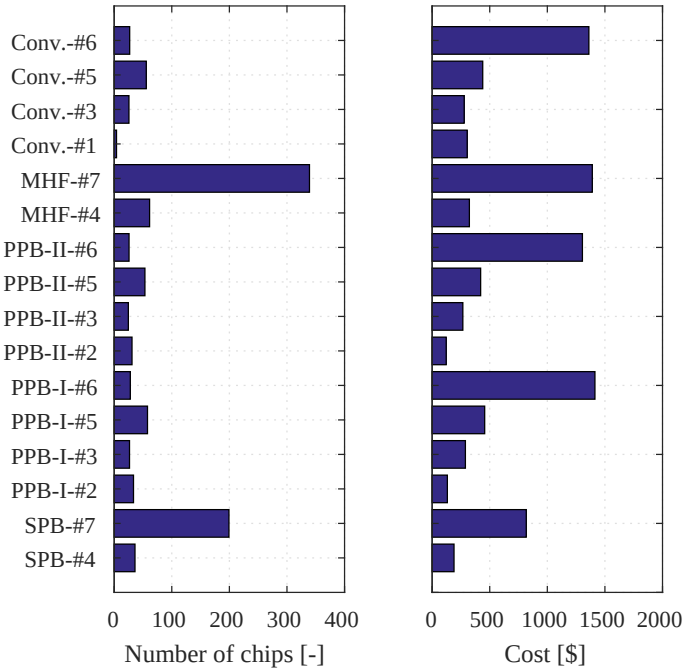

Fig. 16. Number and cost of semiconductor devices required for $A = 3$.

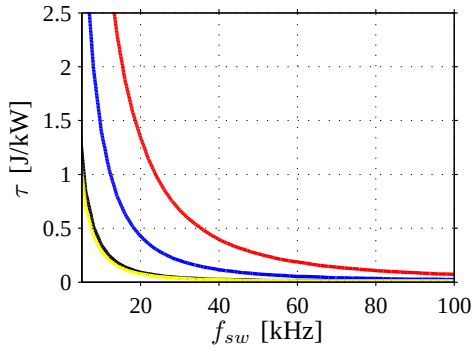

Fig. 17. A comparison of energy storage requirements as a function of switching frequency at 10% peak-to-peak dc current ripple. Red: conventional; black: SPB; blue: PPB-I; yellow: PPB-II.

topologies (excluding the MHF-type converter) when the peak-to-peak battery current ripple is limited to 10% of the current at rated power. Obviously, the energy storage requirement decreases as the switching frequency increases. For the SPB- and PPB-II converters interleaving of the modulation carriers is adopted as described in [18], [22], [38] which significantly reduces the energy storage requirements.

For the MHF-type converter, the second-order harmonic due to the submodules being of single-phase type need to be absorbed by the submodule capacitances. In [14], a closed-form expression of the required submodule capacitance for the MHF-type converter is presented which, assuming a 10 V variation of the submodule capacitor voltages results in an energy storage requirement at rated speed (2800 rpm) and power (30 kW) of around 1 J/kW for machine M3 (used with the MHF-type converter).

D. Cell Redundancy

Post-fault operation following the failure of a single submodule failure can potentially be realized by short circuiting the faulty submodule in the case of the MHF and SPB converters or disconnecting the faulty submodule in the case of the PPB-I and PPB-II converters [53], [54]. In case of a short circuited submodule, the permanent magnets will induce currents in the short circuited submodules. Further, the capacitor-voltage references need to be adjusted so that the voltage is shared evenly also during post-fault operation. For the PPB-I converter, the current angles of the remaining phase-leg current angles need to be shifted for the post-fault operation in the PPB-I converter [16]. Ideally, the residual torque should drop with a factor $((m_{\text{sm}}-1)/m_{\text{sm}})$. However, for the MHF and SPB converters, the braking torque due to the short-circuited submodules will further reduce the residual torque. The cell redundancy in terms of average residual torque during a single submodule failure occurring when the drive operates at rated speed (2800 rpm) and rated power (30 kW) has been computed using JMAG and the results are shown in Fig. 18. Obviously, the average residual torque is highest for the PPB-I converter which utilizes the highest number of submodules (5). It can also be seen that the reduction in residual torque due to the induced short-circuit currents (for the SPB and MHF converters) is relatively small which can, at least partly be attributed to the relatively small rotor saliency of these fault-tolerant designs [45].

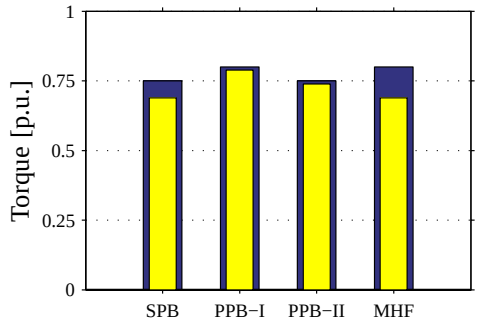

Fig. 18. Residual torque following a single submodule failure for SPB converter (machine M2, 4 submodules), PPB-I converter (machine M3, 5 submodules), PPB-II converter (machine M2, 4 submodules), and MHF converter (machine M3, 5 submodules). Yellow bars: finite-element method; blue bars: ideal case $((m_{\text{sm}}-1)/m_{\text{sm}})$.

E. Cost Comparison

In this section, the material cost of the electric machines and the cost of the semiconductors devices are compared for the five different drive concepts considered. Naturally, such a comparison depends heavily on the assumed material and device costs. Further, costs for gate-drive circuitry (except device #1 in Table IV) or current and voltage sensors are not included. Nevertheless, the obtained figures provide a comparison of costs for the different concepts that could be accompanied when considering other merits of the modular SPB, PPB-I, PPB-II and MHF drive concepts (such as fault tolerance and capacitance requirements) when compared to a conventional two-level three-phase drive.

For the semiconductors, only the devices with the total lowest semiconductor costs in Fig. 16 are considered which excludes the WBG devices. Hence, for the conventional (two-level three-phase) converter, device #3 is considered, for the SPB and MHF converters, device #4 is considered, and for the PPB-I and PPB-II converters device #2 is considered. For the electric machinery, the adopted cost figures are reported in Table V. For all three machine designs reported in Table III, the total magnet price dominates the total cost. Further, the short stack length of the machine with distributed windings (designated M1) results in the smallest machine cost.

TABLE V
ELECTRIC MACHINE MATERIALS COST [44], [55].

Part	Material	Unit	Price
Stator/Rotor Lamination	AK Steel (0.25 mm)	[$/kg]	2.1
Permanent magnets	VACODYM 890 TP	[$/kg]	82.3
Rotor shaft	Copper beryllium alloy	[$/kg]	8.8
Windings	Class H copper	[$/kg]	7.1

The estimated electric machine and semiconductor costs for the five drive concepts are reported in Fig. 19 together with the requirements taken from the FreedomCar 2020 specifications[3].

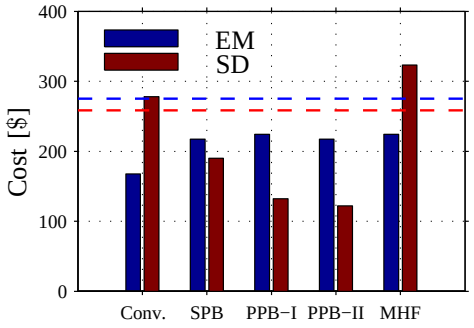

Fig. 19. Cost of the electric machine (EM) and corresponding semiconductor devices (SD) for the five considered concepts. Dashed blue: electric machine unit cost requirement; Dashed red: power electronic cost requirement.

V. CONCLUDING REMARKS

This paper has evaluated recently proposed modular integrated electric drive concepts for automotive traction applications. The evaluation has been presented considering both machine design aspects and the requirements of the corresponding semiconductor switches. The results presented highlight the relative merits and differences that the different modular concepts result into. Key findings are summarized below.

Considering the machine designs, the modular concepts are relatively similar in dimensions and volumes, all having longer stack lengths than the conventional ISDW machine (M1). This indicates that for solutions where the machine

[3]For the semiconductors costs, a 55 kW peak power is assumed yielding a cost limit of $4.7 \cdot 55 = 258.5$ $.

and corresponding converter are not integrated, a conventional distributed winding represents a compact solution, particularly if the axial build of the end winding part can be made short (such as for the welded bar wound winding in [48]). It is further found that the braking torque in the event of a short circuited converter submodule is relatively small for the machines designed for the SPB and MHF converters utilizing series connected submodules. This shows that the post-fault capability for all modular converter concepts are relatively similar and is mainly dependent on the number of submodules utilized.

It is further demonstrated that the capacitor energy storage requirements can be significantly reduced by adopting any of the modular-converter concepts compared to a the two-level three-phase converter. This is an important factor that should be exploited if very hard requirements are put in terms of compactness. The cost comparison indicates that both PPB-type converter topologies potentially can meet the power converter cost requirements since the cost of the semiconductor devices are less than 50% of the FreedomCar 2020 cost requirements enabling the largest margin for the additional costs associated with the power electronics.

Finally, with today's semiconductor technology, replacing the conventional silicon devices with WBG devices would largely increase the total cost. However, the undergoing developments of power semiconductor technology will result in increases market maturity and lowered device prices. Moreover, as the power losses are decreased by using WBG devices, it is possible to optimize the cooling system which would allow for additional reductions in terms of system size and weight. Machine designs not relying little or no amounts of rare-earth based permanent magnets could further contribute to reduce the total system cost.

REFERENCES

[1] A. M. El-Refaie, "Integrated electrical machines and drives: An overview," in *2015 IEEE International Electric Machines Drives Conference (IEMDC)*, May 2015, pp. 350–356.

[2] R. Abebe, G. Vakil, G. L. Calzo, T. Cox, C. Gerada, and M. Johnson, "FEA based thermal analysis of various topologies for integrated motor drives (IMD)," in *Industrial Electronics Society, IECON 2015 - 41st Annual Conference of the IEEE*, Nov 2015, pp. 1976–1981.

[3] J. Wang, Y. Li, and Y. Han, "Evaluation and design for an integrated modular motor drive (IMMD) with GaN devices," in *2013 IEEE Energy Conversion Congress and Exposition*, Sept 2013, pp. 4318–4325.

[4] R. Abebe, G. Vakil, G. L. Calzo, T. Cox, S. Lambert, M. Johnson, C. Gerada, and B. Mecrow, "Integrated motor drives: state of the art and future trends," *IET Electric Power Applications*, vol. 10, no. 8, pp. 757–771, 2016.

[5] "Integral Motors," (Accessed 13-may-2016). [Online]. Available: http://new.abb.com/motors-generators

[6] "VLT DriveMotor FCM 300," (Accessed 13-may-2016). [Online]. Available: http://drives.danfoss.com/products/vlt/decentral-drives-motion-drives-and-gear-motors/vlt-drivemotor-fcm-300/

[7] A. Gkountaras, C. Dinca, A. Giedymin, P. Birgel, U. Schaefer, and S. Dieckerhoff, "Low cost integrated motor-controller drive for an electrical active suspension system," in *Power Electronics and Applications (EPE'14-ECCE Europe), 2014 16th European Conference on*, 2014.

[8] P. Brockerhoff, Y. Burkhardt, K. Egger, and H. Rauh, "Highly integrated drivetrain solution: Integration of motor, inverter and gearing," in *Electric Drives Production Conference (EDPC), 2014 4th International*, 2014.

[9] A. Schmidhofer, J. Horvat, T. Gabriel, H. Lanzenberger, D. Prix, and M. Bichler, "Highly integrated power electronics for a 48 V hybrid drive application," in *Power Electronics and Applications (EPE), 2013 15th European Conference on*, 2013.

[10] H. Shimizu, T. Okubo, S. Ishikawa, and M. Abe, "Development of an integrated electrified powertrain for a newly developed electric vehicle," SAE Technical Paper, Tokyo, Japan, Tech. Rep. 2013-01-1759, Apr. 2013.

[11] Y. Shakweh, G. H. Owen, D. J. Hall, and H. Miller, "Plug and play integrated motor drives," in *Power Electronics, Machines and Drives, 2002. International Conference on (Conf. Publ. No. 487)*, June 2002, pp. 655–661.

[12] N. R. Brown, T. M. Jahns, and R. D. Lorenz, "Power converter design for an integrated modular motor drive," in *Industry Applications Conference, 2007. 42nd IAS Annual Meeting. Conference Record of the 2007 IEEE*, Sept 2007, pp. 1322–1328.

[13] F. Hilpert, K. Brinkfeldt, and S. Arenz, "Modular integration of a 1200 V SiC inverter in a commercial vehicle wheel-hub drivetrain," in *Electric Drives Production Conference (EDPC), 2014 4th International*, 2014.

[14] M. Schulz, L. Lambertz, and R. Marquardt, "Dimensioning of modular high frequency converter for drives," in *ECCE Asia Downunder (ECCE Asia), 2013 IEEE*, June 2013, pp. 675–680.

[15] S. Norrga, L. Jin, O. Wallmark, A. Mayer, and K. Ilves, "A novel inverter topology for compact EV and HEV drive systems," in *Industrial Electronics Society, IECON 2013 - 39th Annual Conference of the IEEE*, Nov 2013, pp. 6590–6595.

[16] L. Jin, S. Norrga, H. Zhang, and O. Wallmark, "Evaluation of a multiphase drive system in EV and HEV applications," in *2015 IEEE International Electric Machines Drives Conference (IEMDC)*, May 2015, pp. 941–945.

[17] G. Engelmann, M. Kowal, and R. W. D. Doncker, "A highly integrated drive inverter using DirectFETs and ceramic dc-link capacitors for open-end winding machines in electric vehicles," in *2015 IEEE Applied Power Electronics Conference and Exposition (APEC)*, March 2015, pp. 290–296.

[18] Y. Han, "Design, modeling, and control of multilevel converter motor drive with modular design and split winding machine," in *2014 IEEE 15th Workshop on Control and Modeling for Power Electronics (COMPEL)*, June 2014.

[19] M. Schilling, U. Schwalbe, and T. Wagner, "Modular integrated machine - inverter system - development of a high current SELV system," in *PCIM Europe 2015*, 2015.

[20] G. J. Su, L. Tang, C. Ayers, and R. Wiles, "An inverter packaging scheme for an integrated segmented traction drive system," in *2013 IEEE Energy Conversion Congress and Exposition*, Sep 2013, pp. 2799–2804.

[21] J. J. Wolmarans, H. Polinder, J. A. Ferreira, and D. Zeilstra, "A fault tolerant drive for high speed permanent magnet machines," in *Power Electronics and Applications (EPE 2011), Proceedings of the 2011-14th European Conference on*, 2011.

[22] L. Jin, S. Norrga, O. Wallmark, and M. N. Harnefors, "Control and modulation of the stacked polyphase bridges inverter," in *2014 IEEE Energy Conversion Congress and Exposition (ECCE)*, Sept 2014, pp. 3023–3029.

[23] E. Grunditz and T. Thiringer, "Performance analysis of current BEVs - based on a comprehensive review of specifications," *IEEE Trans. on Transportation Electrification*, vol. 2, no. 3, pp. 270–289, Sept 2016.

[24] A. Walker, M. Galea, C. Gerada, A. Mebarki, and D. Gerada, "A topology selection consideration of electrical machines for traction applications: Towards the FreedomCar 2020 targets," in *Ecological Vehicles and Renewable Energies (EVER), 2015 Tenth International Conference on*, 2015.

[25] H. Zhang, O. Wallmark, M. Leksell, S. Norrga, M. N. Harnefors, and L. Jin, "Machine design considerations for an MHF/SPB-converter based electric drive," in *IECON 2014 - 40th Annual Conference of the IEEE Industrial Electronics Society*, Oct 2014, pp. 3849–3854.

[26] J. K. Tangudu and T. M. Jahns, "Comparison of interior PM machines with concentrated and distributed stator windings for traction applications," in *2011 IEEE Vehicle Power and Propulsion Conference*, 2011.

[27] A. Walker, M. Galea, C. Gerada, A. Mebarki, and D. Gerada, "Design considerations for high performance traction machines: Aiming for the FreedomCar 2020 targets," in *2015 International Conference on Electrical Systems for Aircraft, Railway, Ship Propulsion and Road Vehicles (ESARS)*, 2015.

[28] F. Magnussen and C. Sadarangani, "Winding factors and joule losses of permanent magnet machines with concentrated windings," in *Electric Machines and Drives Conference, 2003. IEMDC'03. IEEE International*, June 2003, pp. 333–339.

[29] J. Wang, Y. Li, and Y. Han, "Integrated modular motor drive design with GaN power FETs," *IEEE Trans. on Industry Applications*, vol. 51, no. 4, pp. 3198–3207, July 2015.

[30] M. Nikouie, O. Wallmark, L. Jin, L. Harnefors, and H. P. Nee, "DC-link stability analysis and controller design for the stacked polyphase bridges converter," *IEEE Trans. on Power Electronics*, vol. 32, no. 2, pp. 1666–1674, Feb. 2017.

[31] S. Gjerde, P. Olsen, K. Ljokelsoy, and T. Undeland, "Control and fault handling in a modular series-connected converter for a transformerless 100 kV low-weight offshore wind turbine," *IEEE Trans. on Industry Applications*, vol. 50, no. 2, pp. 1094–1105, Mar. 2014.

[32] L. Harnefors, K. Pietiläinen, and L. Gertmar, "Torque-maximizing field-weakening control: design, analysis, and parameter selection," *IEEE Trans. on Industrial Electronics*, vol. 48, no. 1, pp. 161–168, Feb. 2001.

[33] Y. Burkhardt, A. Spagnolo, P. Lucas, M. Zavesky, and P. Brockerhoff, "Design and analysis of a highly integrated 9-phase drivetrain for EV applications," in *2014 International Conference on Electrical Machines (ICEM)*, Sept. 2014, pp. 450–456.

[34] N. Bianchi, S. Bolognani, and M. Dai Pré, "Strategies for the fault-tolerant current control of a five-phase permanent-magnet motor," *IEEE Trans. on Industry Applications*, vol. 43, no. 4, pp. 960–970, July 2007.

[35] M. Ruba and D. Fodorean, "Analysis of fault-tolerant multiphase power converter for a nine-phase permanent magnet synchronous machine," *IEEE Trans. on Industry Applications*, vol. 48, no. 6, pp. 2092–2101, Nov. 2012.

[36] B. C. Mecrow, A. G. Jack, J. A. Haylock, and J. Coles, "Fault-tolerant permanent magnet machine drives," *IEE Proceedings - Electric Power Applications*, vol. 143, no. 6, pp. 437–442, Nov 1996.

[37] E. Levi, R. Bojoi, F. Profumo, H. Toliyat, and S. Williamson, "Multi-phase induction motor drives-a technology status review," *IET Electric Power Applications*, vol. 1, no. 4, pp. 489–516, July 2007.

[38] G.-J. Su and L. Tang, "A segmented traction drive system with a small DC bus capacitor," in *2012 IEEE Energy Conversion Congress and Exposition (ECCE)*, Sept. 2012, pp. 2847–2853.

[39] L. Lambertz, R. Marquardt, and A. Mayer, "Modular converter systems for vehicle applications," in *Emobility - Electrical Power Train, 2010*, 2010.

[40] A. Mayer, C. Rolff, and R. Marquardt, "Control concept and stability considerations of the modular high frequency converter," in *2014 16th European Conference on Power Electronics and Applications (EPE'14-ECCE Europe)*, Aug. 2014.

[41] M. Schulz, R. Marquardt, and A. Mayer, "Optimized control strategy enabling minimized capacitance in modular high frequency converters," in *2014 16th European Conference on Power Electronics and Applications (EPE'14-ECCE Europe)*, Aug. 2014.

[42] E. Carraro, "Design of a permanent magnet synchronous motor according to FreedomCAR specifications," Master's thesis, University of Padova, Padova, 2012.

[43] P. B. Reddy, A. M. El-Refaie, K. K. Huh, J. K. Tangudu, and T. M. Jahns, "Comparison of interior and surface PM machines equipped with fractional-slot concentrated windings for hybrid traction applications," *IEEE Trans. on Energy Conversion*, vol. 27, no. 3, pp. 593–602, Sept 2012.

[44] A. M. El-Refaie, J. P. Alexander, S. Galioto, P. Reddy, K. K. Huh, P. de Bock, and X. Shen, "Advanced high power-density interior permanent magnet motor for traction applications," in *2013 IEEE Energy Conversion Congress and Exposition*, Sept 2013, pp. 581–590.

[45] H. Zhang, O. Wallmark, and M. Leksell, "An iterative FEA-based approach for the design of fault-tolerant IPM-FSCW machines," in *Power Electronics and Applications (EPE'15 ECCE-Europe), 2015 17th European Conference on*, 2015.

[46] A. M. EL-Refaie and T. M. Jahns, "Optimal flux weakening in surface PM machines using fractional-slot concentrated windings," *IEEE Trans. on Industry Applications*, vol. 41, no. 3, pp. 790–800, May 2005.

[47] X. Zhang, R. Qu, H. Chen, and J. Luo, "Analysis of d- and q-axis inductances and saliency ratios in interior permanent magnet machines with fractional-slot concentrated- windings considering harmonic effects," in *Electrical Machines and Systems (ICEMS), 2013 International Conference on*, Oct 2013, pp. 1080–1085.

[48] M. F. Hsieh, Y. C. Hsu, D. G. Dorrell, and K. H. Hu, "Investigation on end winding inductance in motor stator windings," *IEEE Trans. on Magnetics*, vol. 43, no. 6, pp. 2513–2515, June 2007.

[49] K. Ma, A. S. Bahman, S. Beczkowski, and F. Blaabjerg, "Complete loss and thermal model of power semiconductors including device rating information," *IEEE Trans. on Power Electronics*, vol. 30, no. 5, pp. 2556–2569, May 2015.

[50] L. Jin, S. Norrga, and O. Wallmark, "Analysis of power losses in power MOSFET based stacked polyphase bridges converters," in *2016 IEEE 8th International Power Electronics and Motion Control Conference (IPEMC-ECCE Asia)*, May 2016, pp. 3050–3055.

[51] http://octopart.com.

[52] A. Karvonen and T. Thiringer, "Parameter analysis of current and voltageripple in a hybrid vehicle traction system," in *IEMDC'15 - IEEE Electric Machines and Drives Conference*, May 2015, pp. 1838–1845.

[53] H. Zhang, O. Wallmark, and M. Leksell, "On fault tolerance for IPM-FSCW machines adopting a modular converter," in *Electrical Machines and Systems (ICEMS), 2014 17th International Conference on*, Oct 2014, pp. 1633–1638.

[54] H. Zhang and O. Wallmark, "Evaluation of winding arrangements in electric machinery for modular electric drives," in *2016 IEEE 8th International Power Electronics and Motion Control Conference (IPEMC-ECCE Asia)*, May 2016, pp. 2820–2825.

[55] C. Dubar, "Design and analysis of a fault-tolerant fractional slot PMSM for a vehicle application," Ph.D. dissertation, Chalmers University of Technology, Göteborg, Sweden, 2016.